This is the peer-reviewed, final accepted version for American Mineralogist, published by the Mineralogical Society of America.
The published version is subject to change. Cite as Authors (Year) Title. American Mineralogist, in press.
DOI: https://doi.org/10.2138/am-2022-8285. http://www.minsocam.org/

Revision 2

Word Count: 8827

Paragenesis of Li minerals in the Nanyangshan rare-metal pegmatite, Northern China: Toward a generalized sequence of Li crystallization in Li–Cs–Ta-type granitic pegmatites

ZHAOYU YANG, RUCHENG WANG*, XUDONG CHE, LEI XIE, AND HUAN HU

State Key Laboratory for Mineral Deposits Research, School of Earth Sciences and Engineering, Nanjing University, Xianlin University Town, Nanjing 210023, China

ABSTRACT

The Nanyangshan Li–Cs–Ta (LCT) pegmatite is the largest of hundreds of pegmatite dikes in the eastern Qinling orogenic district, North China. The Nanyangshan pegmatite is strongly zoned into a contact zone, border zone, wall zone, intermediate zone and core, with Li mineralization occurring predominantly in the intermediate zone. Inwards through the intermediate zone, Li mineralization is divided into subzones of Spd (spodumene), Mbs (montebrasite), Elb (elbaite), and Lpd (lepidolite). Lithium minerals include spodumene, montebrasite, lithiophilite, elbaite, lepidolite, and possible former petalite. Paragenetic assemblages of Li minerals are variable, with spodumene ± Li-phosphates (montebrasite and

lithiophilite), Fe-rich elbaite, lepidolite and possible former petalite in the Spd subzone; Li-phosphates (main montebrasite and rare lithiophilite) + spodumene + Fe-bearing elbaite + lepidolite in the Mbs subzone; Fe-poor elbaite + lepidolite ± montebrasite in the Elb subzone; and lepidolite ± Fe-poor elbaite in the Lpd subzone. Whole-rock contents of Li_2O, P_2O_5, B_2O_3, and F are consistent with the high contents of various Li minerals. Spodumene was formed first and dominantly from a Li-saturated melt in the Spd subzone (1.66 wt.% Li_2O). This subzone graduates into the P-rich Mbs subzone (3.75 wt.% P_2O_5) with montebrasite gradually succeeds Li aluminosilicates, followed by the appearance of abundant Fe-poor elbaite in the Elb subzone (1.04 wt.% B_2O_3), reflecting the consumption of P in the melt. Lepidolite formed after early-formed Li phases in the F-rich Lpd subzone (2.03 wt.% F), as indicated by replacement textures. Amongst the numerous LCT pegmatites worldwide, the Li mineralization sequence can be suggested as Li-aluminosilicates (commonly spodumene and less commonly petalite) → Li-phosphates (montebrasite–amblygonite and triphylite–lithiophilite) → elbaite → lepidolite, and can be regarded as a general sequence for Li mineralization.

Keywords: spodumene, montebrasite–amblygonite, triphylite–lithiophilite, elbaite, lepidolite, pegmatite zonation

INTRODUCTION

Lithium (Li), as the lightest "energy metal", is widely used in emerging technologies (e.g., rechargeable batteries), nuclear fusion technologies and even medicine (Gourcerol et al. 2019; Bibienne et al. 2020). Natural Li resources are derived mainly from pegmatites and sedimentary rocks as well as evaporative brines. Lithium pegmatites are commonly considered Li–Cs–Ta (LCT)-type pegmatites, which account for 50–60% of global Li production (Bowell et al. 2020; USGS 2021). These pegmatites typically contain a series of primary Li minerals, including spodumene, petalite, lepidolite, elbaite, and montebrasite, with the variable contents of these minerals constituting the basis for distinguishing rare-element pegmatite subtypes, such as spodumene-, petalite-, lepidolite-, elbaite-, and montebrasite-subtype pegmatites (Černý and Ercit 2005). This division reflects the nature of the evolution of Li pegmatites. The spodumene subtype is the most common and produces the largest hard-rock Li deposits, such as the Greenbushes pegmatite in Australia (Linnen et al. 2012), and the Jiajika pegmatite in western China (Huang et al. 2020).

Furthermore, LCT-type pegmatites commonly display complex internal zonation, reflecting the occurrence of complex Li mineral assemblages rather than one dominant Li mineral in the pegmatite. It is commonly noted in the literature that a series of Li minerals (such as aluminosilicates, borosilicates, and phosphates) may be identified in a single pegmatite body. Some studies have shown relationships between different Li phases, such as transformation from petalite to spodumene with

decreasing temperature (London 2008) or an increasing abundance of montebrasite–amblygonite relative to spodumene with enrichment of P_2O_5 in the melt (London and Burt 1982a; London et al. 1999). However, whether a continuous crystallization sequence of Li minerals exists and the main factors controlling the stability of paragenetic Li minerals are still unresolved issues, and such an understanding is now essential because of the high levels of interest in Li exploitation.

The Nanyangshan pegmatite is one of the largest of hundreds of pegmatite dikes in the eastern Qinling orogenic district, North China (Lu et al. 2010). As a typical LCT-type pegmatite, it exhibits strongly developed internal zoning and is extensively mineralized in Li and other rare elements. In this study, we identify a series of Li mineral assemblages in successive internal zones of the pegmatite; i.e., spodumene, montebrasite, lithiophilite, elbaite, lepidolite, and possible former petalite. This pegmatite is therefore a good example of the crystallization sequence of Li minerals. By comparing our results with those from other Li pegmatites worldwide, we can suggest a generalized sequence for the evolution of Li minerals in LCT-type pegmatites.

Geological Background

The Qinling orogen formed as a result of multiple collisions between the North China and South China cratons, involving a history of more than 3 billion years of tectonism, with the effects of collision extending WNW–ESE across central China (Mattauer et al. 1985; Kröner et al. 1993). The Qinling Orogen comprises the Qinling microplate, the Qinling complex, and the Erlangping Group (Fig. 1a; Wang

et al. 2009). The Qinling complex is located between the Shangdan and Zhuxia faults. Granites and associated pegmatites are widely distributed within the Qinling complex, including thousands of pegmatite dikes that form a swarm over an area of 800 km^2 in eastern Qinling (Lu et al. 2010). The pegmatites have been dated at 440 to 380 Ma by multiple geochronological methods (Wang et al. 2009; Zhou et al. 2021). From southeast to northwest, the pegmatites are grouped within four zones: Longquanping, Shangnan, Luanzhuang, and Guanpo. The three former zones contain mainly Be–Nb–Ta mineralization, whereas the Guanpo cluster is dominated by Li–Cs–Nb–Ta mineralization, which appears as spodumene, montebrasite, lithiophilite, elbaite, lepidolite, columbite-group minerals, microlite-group minerals, cassiterite, beryl and pollucite. Among the hundreds of pegmatite dikes in Guanpo, the Nanyangshan pegmatite is a representative dike with clear zonation (Lu et al. 2010).

The Nanyangshan pegmatite is located 2.3 km southwest of Guanpo town (33°52′N, 110°44′E). It forms a vein ~300 m long and 30–80 m wide, showing an overall trend of N 40° E and a dip of 60° to the SE, but rotating at its southern end into an approximately N-S direction with a dip of 60° to the east (Fig. 1b). According to the classification of pegmatites by Černý and Ercit (2005), the Nanyangshan pegmatite belongs to the Li–Cs–Ta (LCT) type. This pegmatite has been mined for Li but is now exploited for mineral specimens of elbaite, spodumene, and lepidolite.

Analytical Methods

Detailed procedures for whole-rock trace-element analyses and for analytical

imaging and major-, minor- and trace-element determinations of minerals are included in the Supplementary Methods.

Whole-rock analysis

Major elements of the border, wall, and intermediate zones (including the Spd, Mbs, Elb, and Lpd subzones) of the Nanyangshan pegmatite were analyzed using a wet chemical technique at the Analysis Center of the No.230 Research Institute of the China National Nuclear Corporation (CNNC), Changsha, China. The method used is as described in the Chinese National standard protocol GB/T 14506-2010DZG93-05. The analytical error for major-element content determinations is below 5%.

Trace-element analyses were conducted at the premises of ALS Minerals–ALS Chemex, Guangzhou, China. Most trace elements were measured with a Perkin Elmer Elan 9000 inductively coupled plasma–mass spectroscopy (ICP–MS) instrument using Li borate ($LiBO_2/Li_2B_4O_7$) fusion. Other metallic elements (Li) were determined by Agilent VISTA ICP–atomic emission spectroscopy (ICP–AES) using Aqua Regia (GEO-AR01) or 4-Acid (GEO-4ACID). The precision control relative deviation (RD%) and accuracy control relative error (RE%) are both <10%.

Imaging and major- and minor-element analyses of minerals

Cathodoluminescence (CL) images of Li aluminosilicates were acquired with a cathodoluminescence CLF-2 instrument coupled to a Leica DM 2700P microscope. Pulse-colored mineral maps, back-scattered electron (BSE) images, and qualitative analyses of minerals were acquired using field emission scanning electron

131 microscopy (FESEM; Zeiss Sigma 300 for mineral maps; Zeiss Supra 55 for BSE
132 images and qualitative analyses). Corresponding quantitative analyses of minerals
133 (spodumene, montebrasite, lithiophilite, elbaite, lepidolite and analcime–
134 pollucite-series) were performed on polished thin sections using a JEOL
135 JXA-8100M electron microprobe (EMP) in wavelength-dispersive mode. Analytical
136 uncertainties are <1% for major elements and <10% for trace elements. All analyses
137 were conducted at the State Key Laboratory for Mineral Deposits Research at
138 Nanjing University, Nanjing, China.

139 **In situ trace-element analyses for lepidolite and elbaite**

140 In situ trace-element analyses for lepidolite and elbaite were conducted by laser
141 ablation-inductively coupled plasma-mass spectrometry (LA–ICP–MS) using a
142 RESOlution S155 LA system coupled with a Thermo Fisher Scientific iCAP–Q ICP–
143 MS instrument at the State Key Laboratory for Mineral Deposits Research at
144 Nanjing University, Nanjing China. Both precision and accuracy are better than ±5%
145 for most of the elements analyzed.

146 # RESULTS

147 **Petrological characteristics of the Nanyangshan pegmatite**

148 The Nanyangshan pegmatite is strongly zoned with respect to variable
149 petrographic characteristics. From contact with the diopside marble inward, the
150 pegmatite can be divided into a contact zone, a border zone, a wall zone, an
151 intermediate zone, and a core (Fig. 1b). Rare-element (Li–Nb–Ta–Cs) mineralization

occurs primarily in the intermediate zone. Study of two prospects in the field followed by identifications of the minerals in the laboratory show that the intermediate zone can be subdivided inwards according to the dominant Li-bearing minerals into spodumene, montebrasite, elbaite, and lepidolite subzones.

The main rock-forming and Li-bearing minerals in each zone are listed in Supplemental Table 1. The contact zone is composed of quartz, albite, K-feldspar, and rare carbonates (calcite and dolomite). In some cases, coarse schorl grains are oriented perpendicular to the boundary with marble. Cassiterite, columbite-group minerals and zircon occasionally occur in the contact zone. The ~1-m-thick border zone comprises mainly fine-grained saccharoidal albite (<200 μm) with minor quartz and muscovite. Rare accessory minerals include cassiterite, columbite-group minerals, zircon and beryl. It has a sharp contact with the wall zone that is marked by an abrupt increase of grain size. The wall zone is up to 2 m thick and consists of coarse-grained (2–5 cm) muscovite, quartz, albite, and accessory schorl. Accessory phases include cassiterite, columbite-group minerals, beryl and zircon.

The subzones of the intermediate zone have distinctive Li mineral(s). The spodumene subzone (Spd subzone) is characterized by quartz (45 vol.%), albite (25 vol.%), tabular coarse-grained (1–5 cm) light-green spodumene (20 vol.%), minor muscovite (5 vol.%), and blue tourmaline (probably elbaite; 4 vol.%) (Fig. 2a–b). Symplectic intergrowths of spodumene and quartz are found locally (<1 vol.%). Other Li minerals (montebrasite, lithiophilite and lepidolite) are also rare (<1 vol.%). The montebrasite subzone (Mbs subzone) consists mostly of quartz (55 vol.%),

This is the peer-reviewed, final accepted version for American Mineralogist, published by the Mineralogical Society of America.
The published version is subject to change. Cite as Authors (Year) Title. American Mineralogist, in press.
DOI: https://doi.org/10.2138/am-2022-8285. http://www.minsocam.org/

coarse-grained (1–4 cm) montebrasite (15 vol.%), and albite (14 vol.%). Spodumene (6 vol.%), green elbaite (6 vol.%), lepidolite (3 vol.%) and lithiophilite (1 vol.%) are also present in the Mbs subzone (Fig. 2c-d). The elbaite subzone (Elb subzone) consists typically of aggregates of pink elbaite (1–8 cm, 16 vol.%), albite (50 vol.%), and quartz (26 vol.%) as major minerals, along with minor lepidolite and accessory montebrasite (8 vol.%; Fig. 2e–f). The lepidolite subzone (Lpd subzone) reveals a complex assemblage of fine-grained albite (35 vol.%) and pink flakes of lepidolite (60 vol.%) with minor quartz (3 vol.%) and elbaite (2 vol.%) (Fig. 2g–h). Other rare metal minerals in the Intermediate zone are cassiterite, columbite-group minerals, microlite-group minerals, Cs-rich beryl, zircon and pollucite. The core is composed exclusively of quartz.

Whole-rock chemistry

Whole-rock compositions of the border, wall, and Li-mineralized intermediate zones (including the Spd, Mbs, Elb, and Lpd subzones) are listed in Supplemental Table 2. Overall, both major- and minor-element contents are within the compositional range of typical LCT-type pegmatites. All zones have low TiO_2 (≤0.02 wt.%), MgO (≤0.05 wt.%), and MnO (≤0.16 wt.%) contents. The contents of total FeO (FeOt) in the intermediate zone show a decreasing trend inward, namely, 0.43 wt.% FeO in the Spd subzone, 0.25 wt.% in the Mbs subzone, 0.14 wt.% in the Elb subzone, and 0.03 wt.% in the Lpd subzone.

Consistent with the high abundance of various Li minerals, the intermediate zone has high Li_2O contents of 1.66 wt.% in the Spd subzone, 2.68 wt.% in the Mbs

196 subzone, 1.13 wt.% in the Elb subzone, and 2.07 wt.% in the Lpd subzone. In
197 addition, volatiles (P_2O_5, B_2O_3, and F) help to distinguish different subzones, with
198 3.75 wt.% P_2O_5 in the Mbs subzone, 1.04 wt.% B_2O_3 in the Elb subzone, and 2.03
199 wt.% F in the Lpd subzone.

200 **Mineralogical features of Li-bearing minerals**

201 Lithium minerals occur mainly in the intermediate zone, which is subdivided
202 inward into the Spd, Mbs, Elb, and Lpd subzones. Lithium minerals include mainly
203 spodumene, montebrasite, elbaite and lepidolite. Lithiophilite and symplectic
204 intergrowths of spodumene with quartz are also rarely observed.

205 **Spodumene**. Spodumene is abundant in the Spd subzone. It is green and lath
206 shaped with grain sizes of around 1–5 cm and is embedded mostly in quartz and
207 albite (Fig. 2a–b). Spodumene becomes rare in the Mbs subzone (Fig. 2c–d) and
208 disappears completely in the Elb subzone. In the Mbs subzone, spodumene grains
209 are white or yellowish in color, measure up to 3 cm in length, and occur in
210 association with quartz and montebrasite.

211 Spodumene has a nearly ideal end-member composition (Supplemental Table 3),
212 except for some slight variation in Fe content. Through the Spd subzone, the FeO
213 content of spodumene (mean 0.42 wt.%) decreases to reach the EMP detection limit
214 ($\leq$0.01 wt.%) in the Mbs subzone.

215 **Spodumene + quartz intergrowths**. At the micrometer scale, fine-grained
216 symplectic intergrowths of spodumene + quartz (SQIs) occur in the Spd subzone
217 (Supplemental Fig. 1). The SQIs commonly show sharp boundaries with contact

minerals such as primary spodumene (Fig. 3) or albite. Fine-grained spodumene in the SQIs contains 0.37 wt.% FeO (Supplemental Table 3). Analcime–pollucite crystals are observed as dendrites following between SQIs and albite (Fig.3d; Supplemental Table 4).

Montebrasite. Montebrasite, the principal Li phosphate mineral in Nanyangshan, occurs only as rare tiny grains in the Spd and Elb subzones but becomes concentrated in the Mbs subzone as large subhedral white crystals (1–4 cm; Fig. 2c–d). Compositionally, the mean F content of montebrasite increases from 1.13 wt. % in the Spd subzone through 3.14 wt.% in the Mbs subzone to 4.98 wt.% in the Elb subzone (Supplemental Table 5).

Lithiophilite. Compared with other Li-containing phases, lithiophilite is much scarcer and only occurs in Spd and Mbs subzones. Lithiophilite is often closely intergrown with montebrasite and occasionally forms discrete grains in albite. EPMA data shows different contents of FeO and MnO contents of lithiophilite in Spd and Mbs subzones (Supplemental Table 6). From Spd to Mbs subzone, the contents of FeO (9.70 wt.% on average to 0.57 wt.% on average) in lithiophilite decrease while the contents of MnO (35.14 wt.% on average to 44.80 wt.% on average) increase.

Elbaite. Tourmaline is widely present in the Nanyangshan pegmatite. However, elbaite is limited to the intermediate zone, including the Spd, Mbs, Elb and Lpd subzones, with various colors, sizes, compositions, and abundances (Supplemental Table 1; Fig. 2). In the Spd subzone, elbaite appears blue in color and occurs as scarce and fine-grained crystals (<1 cm). Elbaite is light green in the Mbs subzone,

240 occurring as a minor constituent with sizes of 1 to 2 cm. Pink elbaite is present in the
241 Elb subzone as abundant aggregates (up to 5 cm), whereas similar pink elbaite is
242 distributed only sporadically in the Lpd subzone. At the micrometer scale, zoned and
243 subhedral elbaite crystals are common in the Spd and Mbs subzones, displaying
244 obvious compositional heterogeneity with faint light cores in the middle part of the
245 subzone (Fig. 4a–b).

246 The composition of elbaite from the Nanyangshan pegmatite is highly variable,
247 particularly in terms of the FeO and Li_2O contents (Fig. 4c; Supplemental Table 7).
248 Major compositional variations include a decrease in Fe concomitant with an
249 increase in Li from the Spd to the Mbs, Elb, and Lpd subzones. The chemical
250 composition of elbaite ranges from Fe-rich elbaite in the Spd subzone (mean 7.16
251 wt.% FeO) through Fe-bearing elbaite in the Mbs subzone (mean 5.04 wt.% FeO) to
252 Fe-poor elbaite in the Elb (mean 0.34 wt.% FeO) and Lpd (mean 0.11 wt.% FeO)
253 subzones. In contrast, mean Li_2O contents in elbaite increase from 1.43 wt.% in the
254 Spd subzone to 1.70 wt.% in the Mbs subzone through 2.18 wt.% in the Elb subzone
255 to 2.56 wt.% in the Lpd subzone. The mean F contents of each subzone are uniform,
256 whereas in Spd (F: 0.47 (0.05)) and Mbs (F: 0.50 (0.07)) subzones, the upper limits
257 of F (apfu) are slightly higher than 0.5; these compositions could qualify as
258 fluor-elbaite.

259 **Lepidolite**. As the principal Li-bearing species of mica, lepidolite occurs
260 throughout in the intermediate zone, being sporadic in the Spd subzone but dominant
261 in the Lpd subzone (Supplemental Table 1). Textural relationships show lepidolite

This is the peer-reviewed, final accepted version for American Mineralogist, published by the Mineralogical Society of America.
The published version is subject to change. Cite as Authors (Year) Title. American Mineralogist, in press.
DOI: https://doi.org/10.2138/am-2022-8285. http://www.minsocam.org/

overgrows earlier formed minerals, e.g., muscovite (Fig. 5a) and spodumene (Fig. 5c), or forms fine-grained and unfoliated aggregates, a typical mode of occurrence, particularly in the Lpd subzone (Fig. 2g-h).

The composition of lepidolite varies according to subzone. Overall, Li_2O and F contents increase simultaneously with a decrease in FeO in lepidolite from the Spd subzone to the Mbs subzone and through the Elb subzone into the Lpd subzone (Fig. 6; Supplemental Table 8). Lepidolite in the Spd subzone contains the highest mean FeO content (2.25 wt.%), which decreases to an average of 0.52 wt.% in the Mbs subzone and <0.10 wt.% in the Elb and Lpd subzones. The mean Li_2O contents of lepidolite increase slightly from 5.22 wt.% in the Spd subzone to 5.99 wt.% in the Mbs subzone, 6.26 wt.% in the Elb subzone, and 6.51 wt.% in the Lpd subzone. The mean F content shows a similar increasing trend from 5.77 wt.% in the Spd subzone to 6.84 wt.% in the Mbs subzone, 6.87 wt.% in the Elb subzone, and 7.22 wt.% in the Lpd subzone.

Discussion

Paragenetic assemblages of Li mineralization in the Nanyangshan pegmatite

Although the Nanyangshan pegmatite is composed of border, wall, intermediate and core zones, Li mineralization is limited mostly to the intermediate zone. Furthermore, Li minerals in the Spd, Mbs, Elb, and Lpd subzones constitute different paragenetic assemblages (Supplemental Table 1; Fig. 7).

Inward through the intermediate zone, the Spd subzone appears first.

283 Spodumene is the dominant Li mineral and SQIs are observed occasionally (Fig. 3).
284 The pre-intergrowth composition of SQIs were estimated by the AF (Area Fraction)
285 method, following the procedure in Supplemental Table 9. The estimated
286 composition is similar to published petalite compositions (Černý and London 1983).
287 We also tested the average compositions of three different SQIs with the beam
288 diameter of 100 μm, and the results are comparable to calculated petalite
289 (Supplemental Table 9). Thus, this symplectic texture could result from the
290 breakdown of a possible former petalite (Černý and Ferguson 1972). Other Li phases
291 are distributed sporadically in the Spd subzone. The assemblage of Li minerals in the
292 Spd subzone is thus spodumene ± Li-phosphates (montebrasite + lithiophilite),
293 Fe-rich elbaite (mean 7.16 wt.% FeO), lepidolite and possible former petalite.

294 In the Mbs subzone, Li aluminosilicates are sharply lower in content compared
295 with the Spd subzone, whereas phosphates (mostly montebrasite) become dominant
296 in addition to the increased abundance of elbaite and lepidolite. The assemblage is
297 established as Li-phosphates (main montebrasite and rare lithiophilite) + spodumene
298 + Fe-bearing elbaite (mean 5.04 wt.% FeO) + lepidolite.

299 Reflecting progressive crystallization, elbaite content increases and becomes the
300 dominant magmatic Li mineral in the Elb subzone. Lepidolite is more concentrated
301 in Elb subzone as one of the rock-forming mineral compared to Spd and Mbs
302 subzones, by contrast, montebrasite only appears sporadically. An assemblage of
303 Fe-poor elbaite (mean 0.34 wt.% FeO) + lepidolite ± montebrasite typifies the Elb
304 subzone.

Lepidolite is abundant in the Lpd subzone and represents the final stage of crystallization of the intermediate zone. Fine purple flakes of lepidolite are widely distributed in the Lpd subzone, whereas elbaite is only rarely observed. An assemblage of lepidolite ± Fe-poor elbaite (mean 0.11 wt.% FeO) is thus the latest assemblage to form in the intermediate zone.

Stability of Li mineral succession in the Nanyangshan pegmatite

Several Li minerals successively crystallized during the different stages of crystallization of the Nanyangshan pegmatite. Variations in pressure and temperature (Stewart 1978; London 1984; Chakoumakos and Lumpkin 1990), fugacities of P, B and F (London and Burt 1982a; Wolf and London 1997; London et al. 1999; Vekstel and Thomas 2002; Munoz 1971; Li et al. 2019), together with Li content (Maneta et al. 2015), are expected to have controlled the succession of Li minerals.

Spodumene and petalite are the most important Li phases in LCT type pegmatites. Melts become saturated in these two minerals only when their Li_2O contents reach 1.08–2.15 wt.% at 500–700 °C (Maneta et al. 2015). Two other Li-aluminosilicates, bikitaite and eucryptite are relatively uncommon and rarely crystallize early; instead these minerals replace existing spodumene or petalite (Grew et al. 2019; London 2017). For the Nanyangshan pegmatite, the outer zones (border and wall zones) are low in Li (mostly <0.10 wt.% Li_2O). However, the Spd subzone has a high Li_2O content (1.66 wt.%) that exceeds the experimentally deduced threshold for triggering the crystallization of spodumene and petalite. This explains the dominant appearance of spodumene in the Spd subzone. In Tanco

(Stilling et al. 2006) and Bikita (Černý et al. 2003) pegmatites, petalite and spodumene are the first phases to crystallize in Li saturated melt. Nonetheless, the early formation of petalite has not been universally reported, such as in Uyköpingsgruvan, Chomogu No.1 and Covas de Barroso pegmatites (Smeds and Černý 1989; Selway et al. 2002; Liu et al. 2020; Charoy et al. 2001). In pegmatites on the Island of Elba, petalite associated with pollucite formed relatively late in the pockets (Pezzotta 2000), which is comparable to Nanyangshan pegmatite. Given the high partition coefficients (7–23) of Cs in fluids (Webster et al. 1989), the Cs−rich mantle (Cs−rich lepidolite and pollucite) in Figure 5d and vein-like analcime−pollucite in Figure 3 suggest interaction with fluids. Wang et al. (2006) implied that Cs−rich fluid could react with albite by the process: $NaAlSi_3O_8$ (albite) + $Cs^+ \rightarrow CsAlSi_2O_8$ (pollucite) + SiO_2 (quartz) + Na^+. In this case, the late metasomatism gave rise to formation of analcime−pollucite along the rims of possible former petalite and albite (Fig. 3d). The sparse occurrence of possible former petalite and its association with analcime−pollucite suggest that the petalite formed during late metasomatic alteration of the Nanyangshan pegmatite. Subsequently, petalite recrystallized to spodumene + quartz intergrowths by the reaction $LiAlSi_4O_{10} = LiAlSi_2O_6 + 2SiO_2$], resulting in pseudomorph of spodumene plus quartz after petalite (London 1984).

Fluxing elements, such as P, B, F, and H_2O, also control the stability of Li minerals. For example, petalite is stable only in low-P_2O_5 melts (P_2O_5 < 0.60 wt.%; London et al. 2017). If sufficient P_2O_5 is added, Li-phosphates will crystallize

instead of petalite and spodumene (e.g., montebrasite and amblygonite: London et al. 1999). This relationship is confirmed in the Nanyangshan pegmatite by the abundance of montebrasite in the P-rich Mbs subzone (3.75 wt.% P_2O_5) as opposed to spodumene in the Spd subzone (0.53 wt.% P_2O_5).

Phosphorous-rich LCT pegmatites are commonly rich in B and show an abundance of elbaite with variable Fe content. Fe-bearing elbaite rarely occurs in the earlier-formed Spd and Mbs subzones. However, Fe-poor elbaite becomes abundant after Li-phosphates has crystallized out, such that it becomes the dominant phase in the Elb subzone (Fig. 7). This could be due to the high P activity, which might reduce the stability of elbaite by lowering the activity of Al in the melt (Wolf and London 1997). The experimental study of Veskler and Thomas (2002) demonstrated that in P- and B-rich melts ($P_2O_5 \approx 5$ wt.%; $B_2O_3 \approx 5$ wt.%), amblygonite crystallized preferentially as the Li phase rather than elbaite. This finding indicates that P (compared with B) is more competitive for Al in the melt, which would favor the crystallization of Li-phosphates first, followed by elbaite.

Another common volatile in LCT pegmatites is F, which generally increases its concentration in the melt with progressive fractional crystallization (London et al. 1989). High activities of F and H_2O favor the precipitation of F-rich lepidolite (London et al. 2017). In addition, F-rich fluids affect the stability of existing Li phases (London and Burt 1982a, b). For example, Li aluminosilicates can be converted to lepidolite in F–H_2O-rich fluids (Munoz 1971; Li et al. 2019). In Nanyangshan, F contents in the remaining melt tended to increase as the pegmatite

crystallized out, reaching their highest values in the Lpd subzone (F = 2.03 wt.%). This is mirrored by the abundant occurrence of lepidolite in the Lpd subzone.

Euhedral and coarse-grained features of spodumene, Li-phosphates (montebrasite and lithiophilite) and elbaite indicate a magmatic origin. Among them, elbaite shows the characteristics of continuous compositional changes (Fig. 4), which could be explained by inward fractional crystallization (Roda-Robles et al. 2015). In contrast, textural evidence of fine-grained lepidolite overgrowing early-formed phases such as muscovite and spodumene and filling in the cracks of elbaite and montebrasite suggest its late-magmatic stage origin (Fig. 5).

Comparisons with typical LCT pegmatites worldwide: Toward a generalized sequence of Li crystallization in LCT-type pegmatites

Currently, LCT pegmatites are the most important field for Li resources as nearly 60% Li resources are extracted from LCT pegmatites (Bowell et al. 2020). These Li pegmatites are distributed worldwide and the species diversity of Li minerals has increased since 3050 Ma (Grew et al. 2019; Grew 2020). The evolution of Li minerals, as recorded by Li aluminosilicates, phosphates, borosilicates, and micas typical of LCT-type pegmatites worldwide, and summarized in Figure 8, is revealed in the Nanyangshan pegmatite.

Some Li-bearing pegmatites are unzoned, such as the Kings Mountain (the largest Li deposit in America) and Jiajika (the largest Li deposit in China) pegmatites, with dominant spodumene being distributed uniformly (Kesler 1961; Chou and Li 2014). However, pegmatites are commonly zoned with the sequential crystallization

of a contact zone, border zone, wall zone, intermediate zone, and core, and even miarolitic cavities or replacement bodies (London 2018). In zoned pegmatites, Li minerals rarely occur in the border or wall zones from the start of crystallization unless the melt is substantially undercooled (Maneta et al. 2015). Most Li minerals occur in the intermediate zone or core after extended (70%–80%) fractional crystallization (Maneta and Baker 2014; London and Morgan 2017). As described in this study, a series of Li minerals characterizes the intermediate zone of the Nanyangshan pegmatite. Some other LCT pegmatites display a similar successive crystallization of Li minerals (Fig. 9).

In the Tanco pegmatite, the Li mineral assemblage changes from Li-aluminosilicates (petalite + spodumene) ± Li-phosphates (montebrasite–amblygonite) ± elbaite in the lower intermediate zone through Li-aluminosilicates (petalite + spodumene) + amblygonite + elbaite in the upper intermediate zone to lepidolite ± elbaite in the central intermediate zone (Stilling et al. 2006). Another typical LCT pegmatite is Koktokay No. 3 (Altai), which has nine zones formed of spodumene in the outer zone (zone 4), spodumene + Li-phosphate (montebrasite + lithiophilite) + elbaite in the inner zones (5 + 6), and lepidolite ± elbaite in the core zones (7 + 8; Zou and Li 2006). For the Bikita and Harding pegmatites, Li mineral types are similar, with Li phases changing from Li-aluminosilicates (spodumene in Harding pegmatite; spodumene + petalite in Bikita pegmatite) in the intermediate zone to lepidolite in the core zone (Černý et al. 2003; Chakoumakos and Lumpkin 1990). In comparison, Li minerals in the Yellowknife pegmatite vary from

spodumene ± Li-phosphate (triphylite) in the intermediate zone through spodumene + Li-phosphate (montebrasite) in the core zone to lepidolite as a replacement phase for primary Li phases (Wise and Černý 1990). The Bob Ingersoll pegmatite contains Li-phosphates (amblygonite ± triphylite–lithiophilite) in the second intermediate zone, elbaite + lepidolite in the third intermediate zone, and lepidolite ± elbaite in the core (Jolliff et al. 1986; 1987), similar to that observed in the Dobrá pegmatite (Černý et al. 1995).

In combination with the Li minerals identified in these pegmatites, it is worth noting that the LCT-type pegmatites display an idealized, and thus probably generalized, model of paragenetic evolution of Li minerals as Li-aluminosilicates (generally spodumene and less commonly petalite) → Li-phosphates (montebrasite–amblygonite and triphylite–lithiophilite) → elbaite → lepidolite. The large-scale crystallization of petalite is not as common as spodumene in the magmatic stage, as petalite of magmatic origin has been indicated to form only within a narrow range of low P and high T (200–300 MPa, 600–660 °C: London 1984) and spodumene is becoming predominant with continuous decline of temperature and pressure, following the succession of petalite + quartz → spodumene + quartz (London 2017). Certainly, strong hydrothermal activity during the latter stages of crystallization could also result in the occurrence of metasomatic/secondary Li minerals, such as the scarce possible former petalite in Nanyangshan pegmatite and eucryptite in pegmatites from Northern Portugal (Charoy et al. 2001).

IMPLICATIONS

As a typical LCT pegmatite dike and the largest of hundreds in the eastern Qinling orogenic district, North China, the Nanyangshan pegmatite is strongly mineralized with respect to Li in the form of spodumene, montebrasite, lithiophilite, elbaite, lepidolite, and possible former petalite. In particular, these lithium minerals crystallized successively and regularly out over a series of stages. Spodumene ± Li-phosphates (montebrasite and lithiophilite), Fe-rich elbaite and lepidolite formed first in the Spd subzone, followed by Li-phosphates (main montebrasite and rare lithiophilite) + spodumene + Fe-bearing elbaite + lepidolite in the Mbs subzone secondly, Fe-poor elbaite + lepidolite ± montebrasite in Elb subzone thirdly and lepidolite ± Fe-poor elbaite formed in the Lpd subzone lastly.

Through comparing with other LCT pegmatites worldwide, we found typical LCT pegmatites are seen to display successive crystallization sequences of Li minerals similar to that determined in the Nanyangshan pegmatite, following the crystallization sequence of primary lithium minerals as Li-aluminosilicates (generally spodumene, less commonly petalite) → Li-phosphates (montebrasite−amblygonite, triphylite−lithiophilite) → elbaite → lepidolite. During the late hydrothermal or metasomatic stage of pegmatite crystallization, Li-rich fluids could affect primary lithium phases and/or result in the occurrence of metasomatic/secondary Li minerals.

In addition to P-T conditions, this successive sequence of Li minerals is especially controlled by Li, P, B, and F. These elements create a boundary layer of

459 melt that is much more fractionated, adjacent to the crystal surface (e.g., muscovite
460 and schorl) during constitutional zone refining (London 2018). The generalized
461 sequence of lithium minerals could provide constraints for the constitutional zone
462 refining process in LCT pegmatites. As the LCT-type pegmatites account for nearly
463 60% of the global Li production (Bowell et al. 2020), the results in this study
464 provide the guiding significance for Li exploitation.

465 ## ACKNOWLEDGMENTS

466 This study was financially supported by the National Natural Science
467 Foundation of China (Grant No. 91855209), the Fundamental Research Funds for
468 the Central Universities (Grant No. 14380099）, the Key deployment project of the
469 Institute of Geology and Geophysics, Chinese Academy of Sciences (Grant No.
470 IGGCAS-201902). We are indebted to Daniel E. Harlov from the German Research
471 Centre for Geosciences for his constructive criticism and suggestions. We sincerely
472 thank Jiankang Li from the Chinese Academy of Geological Sciences for supporting
473 us of sampling. We are also grateful to the two reviewers, M. Van Lichtervelde, and
474 A. Lima for their helpful comments. We wish particularly to thank the Associate
475 Editor, Edward S. Grew for bringing his considerable expertise with patience to bear
476 on important details and points of clarification.

477 ## REFERENCES CITED

478 Akoh, J.U., Ogunleye, P.O. and Ibrahim, A.A. (2015) Geochemical evolution of
479 micas and Sn-, Nb-, Ta- mineralization associated with the rare metal pegmatite
480 in Angwan Doka, central Nigeria. Journal of African Earth Sciences, 112, 24−36.
481 Anderson, M.O., Lentz, D.R., McFarlane, C.R.M. and Falck, H. (2013) A geological,

geochemical and textural study of a LCT pegmatite: implications for the magmatic versus metasomatic origin of Nb−Ta mineralization in the Moose II pegmatite, northwest Territories, Canada. Journal of Geosciences, 58, 299−320.

Badanina, E.V., Sitnikova, M.A., Gordienko, V.V., Melcher, F., Gäbler, H.-E., Lodziak, J. and Syritso, L.F. (2015) Mineral chemistry of columbite–tantalite from spodumene pegmatites of Kolmozero, Kola Peninsula (Russia). Ore Geology Reviews, 64, 720−735.

Baldwin, J.R., Hill, P.G., Finch, A.A., Knorring, O.V. and Oliver, G.J.H. (2005) Microlite-manganotantalite exsolution lamellae: evidence from rare-metal pegmatite, Karibib, Namibia. Mineralogical Magazine, 69, 917−935.

Bibienne, T., Magnan, J.-F., Rupp, A. and Laroche, N. (2020) From Mine to Mind and Mobiles: Society's Increasing Dependence on Lithium. Elements, 16, 265−270.

Bowell, R.J., Lagos, L., de los Hoyos, C.R. and Declercq, J. (2020) Classification and Characteristics of Natural Lithium Resources. Elements, 16, 259−264.

Burnham, C.W. and Nekvasil, H. (1986) Equilibrium properties of granite pegmatite magmas. American Mineralogist, 71, 239−263.

Bynoe, L. (2014) Shear zone influence on the emplacement of a giant pegmatite, Quebec Canada, 59p. Master thesis. The University of Western Ontario, London.

Černý, P. and Ercit, T.S. (2005) The classification of granitic pegmatites revisited. The Canadian Mineralogist, 43, 2005−2026.

Černý, P. and Ferguson, R.B. (1972) The Tanco pegmatite at Bernic Lake, Manitoba. IV. Petalite and spodumene relations. Canadian Mineralogist, 11, 660−678.

Černý, P. and London, D. (1983) Crystal chemistry and stability of petalite. Tschermaks Mineralogische Und Petrographische Mitteilungen, 31, 81−96.

Černý, P., Anderson, A.J., Tomascak, P.B. and Chapman, R. (2003) Geochemical and morphological features of beryl from the Bikita granitic pegmatite, Zimbabwe. The Canadian Mineralogist, 41, 1003−1011.

Černý, P., Chapman, R., Chackowsky, L.E. and Ercit, T.S. (1989) A ferrotantalite-ferrotapiolite intergrowth from Spittal a.d. Drau, Carinthia, Austria. Mineralogy and Petrology, 41, 53−63.

Černý, P., Chapman, R., Ferreira, K. and Smeds, S.-A. (2004) Geochemistry of oxide minerals of Nb, Ta, Sn, and Sb in the Varuträsk granitic pegmatite, Sweden: The case of an "anomalous" columbite-tantalite trend. American Mineralogist, 89, 505−518.

Černý, P., Staněk, J., Novák, M., Baadsgaard, H., Rieder, M., Ottolini, L., Kavalová, M. and Chapman, R. (1995) Geochemical and structural evolution of micas in the Rožná and Dobrá Voda pegmatites, Czech Republic. Mineralogy and Petrology, 55, 177−201.

Chakoumakos, B.C. and Lumpkin, G.R. (1990) Pressure-temperature constraints on the crystallization of the Harding pegmatite, Taos Country, New Mexico. Canadian Mineralogist, 28, 287−298.

Charoy, B., Noronha, F. and Lima, A. (2001) Spodumene-petalite-eucryptite: Mutual relationships and pattern of alteration in Li-rich aplite-pegmatite dykes from northern Portugal. The Canadian Mineralogist, 39, 729−746.

Chou, I.M. and Li, J. (2014) Studies of silicate melt inclusions in quartz and crystal-rich inclusions in spodumene from Jiajika granitic pegmatite rare-metal deposit in China. Geol. Soc. Am. Abstracts Programs, 46, 696.

Dittrich, T., Seifert, T. and Schulz, B. (2014) Geology, mineralogy and geochemistry of the Mount Deans pegmatite field, Eastern Yilgarn Craton/Australia. Geophysical Research Abstracts, 16, 6577.

Galliski, M.A., Černý, P., Márquez-Zavalía, M.F. and Chapman, R. (1999) Ferrotitanowodginite, $Fe^{2+}TiTa_2O_8$, a new mineral of the wodginite group from the San Elías pegmatite, San Luis, Argentina. American Mineralogist, 84, 773−777.

Galliski, M.A., Marquez-Zavalía, M.F., Černý, P., Martínez, V.A. and Chapman, R. (2008) The Ta-Nb-Sn-Ti oxide-mineral paragenesis from La Viquita, a spodumene-bearing rare-element granitic pegmatite, San Luis, Argentina. The Canadian Mineralogist, 46, 379−393.

Gourcerol, B., Gloaguen, E., Melleton, J., Tuduri, J. and Galiegue, X. (2019) Re-assessing the European lithium resource potential – A review of hard-rock resources and metallogeny. Ore Geology Reviews, 109, 494−519.

Grew, E.S. (2020) The Minerals of Lithium. Elements, 16, 235−240.

Grew, E.S., Bosi, F., Ros, L., Kristiansson, P., Gunter, M.E., Hålenius, U., Trumbull, R.B. and Yates, M.G. (2018) Fluor-elbaite, lepidolite and Ta–Nb oxides from a pegmatite of the 3000 Ma Sinceni Pluton, Swaziland: evidence for lithium–cesium–tantalum (LCT) pegmatites in the Mesoarchean. European Journal of Mineralogy, 30, 205−218.

Grew, E.S., Hystad, G., Toapanta, M.P.C., Eleish, A., Ostroverkhova, A., Golden, J. and Hazen, R.M. (2019) Lithium mineral evolution and ecology: comparison with boron and beryllium. European Journal of Mineralogy, 31, 755−774.

Henry, D.J., Novák, M., Hawthorne, F.C., Ertl, A., Dutrow, B.L., Uher, P. and Pezzotta, F. (2011) Nomenclature of the tourmaline-supergroup minerals. American Mineralogist, 96, 895−913.

Huang, T., Fu, X.F., Ge, L.Q., Wang, D.H., Zou, F.G., Xiao, R.Q., Yang, R. and Fan, J.B. (2020) The genesis of giant lithium pegmatite veins in Jiajika, Sichuan, China: insights from geophysical, geochemical as well as structural geology approach. Ore Geology Reviews, 124, 103557.

Hulsbosch, N. and Muchez, P. (2020) Tracing fluid saturation during pegmatite differentiation by studying the fluid inclusion evolution and multiphase cassiterite mineralisation of the Gatumba pegmatite dyke system (NW Rwanda). Lithos, 354-355, 105285.

Jolliff, B.L., Papike, J.J. and Shearer, C.K. (1986) Tourmaline as a recorder of pegmatite evolution Bob Ingersoll pegmatite, Black Hills, South Dakota. American Mineralogist, 71, 472−500.

Jolliff, B.L., Papike, J.J. and Shearer, C.K. (1987) Fractionation trends in mica and tourmaline as indicators of pegmatite internal evolution: Bob Ingersoll pegmatite, Black Hills, South Dakota. Geochimica Et Cosmochimica Acta, 51, 519−534.

Kesler, S.E., Gruber, P.W., Medina, P.A., Keoleian, G.A., Everson, M.P. and Wallington, T.J. (2012) Global lithium resources: Relative importance of pegmatite, brine and other deposits. Ore Geology Reviews, 48, 55−69.

Kesler, T.L. (1961) Exploration of the Kings Mountain pegmatites. Mining Engineerin. 13(9), 1062−1068.

Kröner, A., Zhang, G.W. and Sun, Y. (1993) Granulites in the Tongbai Area, Qinling Belt, China: Geochemistry, petrology, single zircon geochronology, and implications for the tectonic evolution of eastern Asia. Tectonics, 12, 245−255.

Kuznetsova, L.G. and Prokof'ev, V.Y. (2009) Petrogenesis of extremely lithium-rich spodumene aplites of the Tastyg deposit, Sangilen Highland, Tyva Republic. Doklady Earth Sciences, 429, 1262−1266.

Lagache, M. and Quéméneur, J. (1997) The Volta Grande pegmatites, Minas Gerais, Brazil: An example of rare-element granitic pegmatites exceptiionally enriched in lithium and rubidium. The Canadian Mineralogist, 35, 153−165.

Lazić, B., Kahlenberg, V., Vulić, P., Pešić, L. and Dimitrijević, R. (2009) Meta-autunite from a Li-pegmatite of the Cer Mt., Serbia: Its mineralogical and XRD investigations. Neues Jahrbuch für Mineralogie-Abhandlungen, 186, 333−344.

Li, J.K., Liu, C.Y., Liu, X., Li, P., Huang, Z.B. and Zhou, F.C. (2019) Tantalum and niobium mineralization from F- and Cl-rich fluid in the lepidolite-rich pegmatite from the Renli deposit in northern Hunan, China: Constraints of fluid inclusions and lepidolite crystallization experiments. Ore Geology Reviews, 115, 103187.

Li, P., Li, J.K., Liu, X., Li, C., Huang, Z.B. and Zhou, F.C. (2020) Geochronology and source of the rare-metal pegmatite in the Mufushan area of the Jiangnan orogenic belt: A case study of the giant Renli Nb–Ta deposit in Hunan, China. Ore Geology Reviews, 116, 103237.

Linnen, R.L., Van Lichtervelde, M. and Černý, P. (2012) Granitic pegmatites as sources of strategic metals. Elements, 8, 275−280.

Liu, C., Wang, R.C., Wu, F.Y., Xie, L., Liu, X.C., Li, X.K., Yang, L. and Li, X.J.

(2020) Spodumene pegmatites from the Pusila pluton in the higher Himalaya, South Tibet: Lithium mineralization in a highly fractionated leucogranite batholith. Lithos, 358-359, 105421.

Liu, Y.S., Hu, Z.C., Gao, S., Günther, D., Xu, J., Gao, C.G. and Chen, H.H. (2008) In situ analysis of major and trace elements of anhydrous minerals by LA-ICP-MS without applying an internal standard. Chemical Geology, 257, 34−43.

London, D. (1984) Experimental phase equilibria in the system LiAlSiO4-SiO2-H2O: a petrogenetic grid for lithium-rich pegmatites. American Mineralogist, 69, 995−1004.

London, D. (2008) Pegmatites. Canadian Mineralogist special publication 10.

London, D. (2017) Reading Pegmatites: Part 3—What Lithium Minerals Say. Rocks & Minerals, 92, 144−157.

London, D. (2018) Ore-forming processes within granitic pegmatites. Ore Geology Reviews, 101, 349−383.

London, D. and Burt, D.M. (1982a) Alteration of spodumene, montebrasite and lithiophilite in pegmatites of the White Picacho District, Arizona. American Mineralogist, 67, 97−113.

London, D. and Burt, D.M. (1982b) Chemical models for lithium aluminosilicate stabilities in pegmatites and granites. American Mineralogist, 67, 494−509.

London, D. and Morgan, G.B. (2017) Experimental Crystallization of the Macusani Obsidian, with Applications to Lithium-rich Granitic Pegmatites. Journal of Petrology, 58, 1005−1030.

London, D., Morgan, G.B. and Hervig, R.L. (1989) Vapor-undersaturated experiments with Macusani glass + H_2O at 200 MPa, and the internal differentiation of granitic pegmatites. Contributions to Mineralogy and Petrology, 102, 1−17.

London, D., Wolf, M.B., VI, G.B.M. and Garrido, M.G. (1999) Experimental silicate-phosphate equilibria in peraluminous granitic magmas, with a case study of the Alburqueque batholith at Tres Arroyos, Badajoz, Spain. Journal of Petrology, 40, 215−240.

Lu, X.X., Zhu, C.H., Gu, D.M., Zhang, H.M., Wu, M. and Wu, Y. (2010) The main geological and metallogenic characteristics of granitic pegamtite in Eastern Qinling Belt (in English with Chinese abstract). Geological Review, 56, 21−30.

Maneta, V. and Baker, D.R. (2014) Exploring the effect of lithium on pegmatitic textures: An experimental study. American Mineralogist, 99, 1383−1403.

Maneta, V., Baker, D.R. and Minarik, W. (2015) Evidence for lithium-aluminosilicate supersaturation of pegmatite-forming melts. Contributions to Mineralogy and Petrology, 170, 1−16.

Marchal, K.L., Simmons, W.B., Falster, A.U., Webber, K.L. and Roda-Robles, E.

(2014) Geochemistry, mineralogy, and evolution of Li-Al micas and feldspars from the Mount Mica pegmatite, Maine, USA. The Canadian Mineralogist, 52, 221−233.

Matsubara, S., Kato, A. and Matsuyama, F. (1995) Nb-Ta minerals in a lithium pegmatite from Myokenzan, Ibaraki Prefecture, Japan. Mineralogical Journal, 17, 338−345.

Mattauer, M., Matte, P., Malavieille, J., Tapponnier, P., Maluski, H., Xu, Z.Q., Lu, Y.L. and Tang, Y.Q. (1985) Tectonics of the Qinling Belt: build-up and evolution of eastern Asia. Nature, 317, 496−500.

Mohammedyasin, M.S. (2017) Geology, geochemistry and geochronology of the Kenticha rare metal granite pegmatite, Adola Belt, Southern Ethiopia: A Review. International Journal of Geosciences, 8, 46−64.

Munoz, J.L. (1971) Hydrothermal stability relations of synthetic lepidolite. The American Mineralogist, 56, 2069−2087.

Novák, M. and Černý, P. (1998) Niobium-tantalum oxide minerals from complex granitic pegmatites in the Moldanubicum, Czech Republic: Primary versus secondary compositional trends. The Canadian Mineralogist, 36, 659−672.

Novák, M., Cempírek, J., Gadas, P., Škoda, R., Vašinová Galiová, M., Pezzotta, F. and Groat, L.A. (2015) Boralsilite and Li,Be-bearing "boron mullite" $Al_8B_2Si_2O_{19}$, breakdown products of spodumene from the Manjaka pegmatite, Sahatany Valley, Madagascar. The Canadian Mineralogist, 53, 357−374.

Oyarzábal, J., Galliski, M.Á. and Perino, E. (2008) Geochemistry of K-feldspar and muscovite in rare-element pegmatites and granites from the Totoral pegmatite field, San Luis, Argentina. Resource Geology, 59, 315−329.

Pal, D.C., Mishra, B. and Bernhardt, H.-J. (2007) Mineralogy and geochemistry of pegmatite-hosted Sn-, Ta–Nb-, and Zr–Hf-bearing minerals from the southeastern part of the Bastar-Malkangiri pegmatite belt, Central India. Ore Geology Reviews, 30, 30−55.

Partington, G.A. and McNaughton, N.J. (1995) A review of the geology, mineralization, and geochronology of the greenbushes pegmatite, Western Australia. Economic Geology, 90, 616−635.

Peretyazhko, I.S., Zagorsky, V.Y., Smirnov, S.Z. and Mikhailov, M.Y. (2004) Conditions of pocket formation in the Oktyabrskaya tourmaline-rich gem pegmatite (the Malkhan field, Central Transbaikalia, Russia). Chemical Geology, 210, 91−111.

Peters, S.G. (2011) Summaries of Important Areas for Mineral Investment and Production Opportunities of Nonfuel Minerals in Afghanistan, chapter 5A. USGS.

Pezzotta, F. (2000) Internal structures, parageneses and classification of the

miarolitic Li-bearing complex pegmatites of Elba Island (Italy). Memorie della Societá di Scienze Naturali e del Museo Civico di Storia Naturale di Milano 30, 29–43.

Potter, E.G., Taylor, R.P., Jones, P.C., Lalonde, A.E., Pearse, G.H.K. and Rowe, R. (2009) Sokolovaite and evolved lithian micas from the Eastern Moblan granitic pegmatite, Opatica Subprovince, Quebec, Canada. The Canadian Mineralogist, 47, 337−349.

Qin, K.Z., Zhou, Q.F., Tang, D.M., and Wang, C.L. (2019) Types, internal structural patterns, mineralization and prospects of rare-element pegmatites in East Qinling Mountain in comparison with features of Chinese Altay (in English with Chinese abstract). Mineral Deposits, 38(5), 970−982.

Rao, C., Wang, R.C., Yang, Y.Q., Hatert, F., Xia, Q.K., Yue, X.G. and Wang, W.M.Y. (2017) Insights into post-magmatic metasomatism and Li circulation in granitic systems from phosphate minerals of the Nanping No. 31 pegmatite (SE China). Ore Geology Reviews, 91, 864−876.

Rijks, H.R.P. and van der Veen, A.H. (1972) The geology of the tin-bearing pegmatites in the eastern part of the Kamativi district, Rhodesia. Mineralium Deposita, 7, 383−395.

Roda-Robles, E., Pesquera, A., Gil-Crespo, P.P., Vieira, R., Lima, A., Garate-Olave, I., Martins, T. and Torres-Ruiz, J. (2016) Geology and mineralogy of Li mineralization in the Central Iberian Zone (Spain and Portugal). Mineralogical Magazine, 80, 103−126.

Roda-Robles, E., Simmons, W., Pesquera, A., Gil-Crespo, P.P., Nizamoff, J. and Torres-Ruiz, J. (2015) Tourmaline as a petrogenetic monitor of the origin and evolution of the Berry-Havey pegmatite (Maine, U.S.A.). American Mineralogist, 100, 95−109.

Seltmann, R., Soloviev, S., Shatov, V., Pirajno, F., Naumov, E. and Cherkasov, S. (2010) Metallogeny of Siberia: tectonic, geologic and metallogenic settings of selected significant deposits*. Australian Journal of Earth Sciences, 57, 655−706.

Selway, J.B., Černý, P. and Hawthorne, F.C. (2000) The Tanco pegmatite at Bernic Lake, Manitoba. XIV. Internal tourmaline. The Canadian Mineralogist, 38, 877−891.

Selway, J.B., Smeds, S.-A., Černý, P. and Hawthorne, F.C. (2002) Compositional evolution of tourmaline in the petalite-subtype Nyköpingsgruvan pegmatites, Utö, Stock-holm archipelago, Sweden. Geol. Foren. Forh., 124, 93−102.

Shigley, J.E. and Brown, G.E. (1985) Occurrence and alteration of phosphate minerals at the Stewart Pegmatite, Pala District, San Diego County, California. American Mineralogist, 70, 395−408.

Sirbescu, M.-L.C., Leatherman, M.A., Student, J.J. and Beehr, A.R. (2009) Apatite Textures and compositions as records of crystallization processes in the Animikie Red Ace pegmatite dike, Wisconsin, USA. The Canadian Mineralogist, 47, 725−743.

Smeds, S.-A. and Černý, P. (1989) Pollucite from the Proterozoic petalite-bearing pegamtites of Utö, Stockholm archipelago, Sweden. Geol. Foren. Forh., 111, 361−371.

Sokol, E.V., Seryotkin, Y.V. and Bul'bak, T.A. (2010) Na-Li-Be-rich cordierite from the Murzinka pegmatite field, Middle Urals, Russia. European Journal of Mineralogy, 22, 565−575.

Stewart, D.B. (1978) Petrogenesis of lithium-rich pegmatites. American Mineralogist, 64, 970−980.

Stilling, A., Černý, P. and Vanstone, P.J. (2006) The Tanco pegmatite at Bernic Lake, Manitoba. XVI. Zonal and bulk compositions and their petrogenetic significance. The Canadian Mineralogist, 44, 599−623.

Suwimonprecha, P., Černý, P. and Friedrich, G. (1995) Rare metal mineralization related to granites and pegmatites, Phuket, Thailand. Economic Geology, 90, 603−615.

Sweetapple, M.T., Cornelius, H. and Collins, P.L.F. (2001) Tantalum mineralization of the Wodgina pegmatite district: The Wodgina and Mt. Cassiterite pegmatite orebodies. Excursion guide for Pilbara Metallogeny. Geol. Surv. W.A., Record, 11, 42−58.

Sweetapple, M.T., Grigson, M.W., Tornatora, P. and Urgine, S. (2019) The Archean Mt. Cattlin spodumene pegmatite group and 3D geochemical mapping of large “unzoned” pegmatites of economic significance. The Canadian Mineralogist, 57, 803−805.

Thomas, R.J., Bühmann, D., Bullen, W.D., Scogings, A.J. and De Bruin, D. (1994) Unusual spodumene pegmatites from the Late Kibaran of southern Natal, South Africa. Ore Geology Reviews, 9, 161−182.

Tindle, A.G. and Breaks, F.W. (2000) Columbite-tantalite mineral chemistry from rare-element granitic pegmatites: Separation Lake area, N.W. Ontario, Canada. Mineralogy and Petrology, 70, 165−198.

Tonarini, S., Dini, A., Pezzotta, F. and Leeman, W.P. (1998) Boron isotopic composition of zoned (schorl-elbaite) tourmalines, Mt. Capanne Li-Cs pegmatites, Elba (Italy). European Journal of Mineralogy, 10, 941−952.

U.S. Geological Survey (2021) Lithium in 2019, tables-only release [Online]. Available: https://www.usgs.gov/media/files/lithium-2019-tables-only-release.

Veksler, I.V. and Thomas, R. (2002) An experimental study of B-, P- and F-rich synthetic granite pegmatite at 0.1 and 0.2 GPa. Contributions to Mineralogy and

Petrology, 143, 673−683.

Viana, R.R., Jordt-Evangelista, H. and Stern, W.B. (2007) Geochemistry of muscovite from pegmatites of the Eastern Brazilian pegmatite province: a clue to petrogenesis and mineralization potential. European Journal of Mineralogy, 19, 745−755.

Wang, R.C., Hu, H., Zhang, A.C., Fontan, F., Zhang, H. and Parseval, P.D. (2006) Occurrence and late re-equilibration of pollucite from the Koktokay no. 3 pegmatite, Altai, northwestern China. American Mineralogist, 91, 729−739.

Wang, T., Wang, X.X., Tian, W., Zhang, C.L., Li, W.P. and Li, S. (2009) North Qinling Paleozoic granite associations and their variation in space and time: Implications for orogenic processes in the orogens of central China. Science in China, 52, 1359−1384.

Webster, J.D., Holloway, J.R. and Hervig, R.L. (1989) Partitioning of lithophile trace elements between H_2O and H_2O+CO_2 fluids and topaz rhyolite melt. Economic Geology, 84, 116−134.

Whitworth, M.P. and Rankin, A.H. (1989) Evolution of fluid phases associated with lithium pegmatites from SE Ireland. Mineralogical Magazine, 53, 271−284.

Wise, M.A. and Černý, P. (1990) Primary compositional range and alteration trends of microlite from the Yellowknife pegmatite field, northwest Territories, Canada. Mineralogy and Petrology, 43, 83−98.

Wolf, M.B. and London, D. (1997) Boron in granitic magmas: stability of tourmaline in equilibrium with biotite and cordierite. Contributions to Mineralogy and Petrology, 130, 12−30.

Yang, Y.D., Li, J.Y., Zhu, Y.P. and Liu, J.Y. (2020) Geological characteristics of a pegmatite niobium and tantalum deposit in the east of Manono, Congo (Kinshasa) (in English with Chinese abstract). Mineral Exploration, 11, 1428−1435.

Yin, R., Huang, X.L., Xu, Y.G., Wang, R.C., Wang, H., Yuan, C., Ma, Q., Sun, X.M. and Chen, L.L. (2020) Mineralogical constraints on the magmatic–hydrothermal evolution of rare-elements deposits in the Bailongshan granitic pegmatites, Xinjiang, NW China. Lithos, 352−353.

Zhou, Q., Qin, K. and Tang, D. (2021) Mineralogy of columbite-group minerals from the rare-element pegmatite dykes in the East-Qinling orogen, central China: Implications for formation times and ore genesis. Journal of Asian Earth Sciences, 218, 104879.

Zou, T.R. and Li, Q.C. (2006) Rare and rare earth metallic deposits in Xinjiang, China, 40p (in English with Chinese abstract). Geological Publishing House, Beijing.

FIGURE CAPTIONS

Fig. 1. (a) Distribution of pegmatites in eastern Qinling, modified after Lu et al. (2010) and Qin et al. (2019). (b) Schematic diagram of the textural zones of the Nanyangshan pegmatite. Spd subzone: Spodumene subzone; Mbs subzone: Montebrasite subzone; Elb subzone: Elbaite subzone; Lpd subzone: Lepidolite subzone.

Fig. 2. Hand specimen photographs and mineral maps of the Spd (a–b), Mbs (c–d), Elb (e–f), and Lpd (g–h) subzones.

Abbreviations: Spd (spodumene); Mbs (montebrasite); Elb (elbaite); Lpd (lepidolite); Ms (muscovite); Ab (albite); Qz (quartz); Ap (apatite).

Fig. 3. Symplectic spodumene + quartz intergrowths (SQIs) in the Spd subzone. (a) Colored image; (b) photomicrograph with outline of (c) and (d); (c) cathodoluminescence image; (d) BSE image of vein-like analcime–pollucite developed at the contact between albite and SQIs.

Abbreviations: Spd (spodumene); Pol (pollucite); Lpd (lepidolite); Ms (muscovite); Qz (quartz); Ab (albite); Anl (analcime); SQIs (spodumene + quartz intergrowths).

Fig. 4. (a–b) Backscattered electron images of single zoned elbaite crystal in the Spd subzone (a) and Mbs subzone (b); (c) Classification of tourmaline in different subzones (after Henry et al. 2011).

Abbreviations: Elb (elbaite); Lpd (lepidolite); Ab (albite); Qz (quartz).

Fig. 5. Backscattered electron images of lepidolite. (a) Lepidolite rimming muscovite in the Spd subzone; (b) lepidolite with relics of muscovite in the Lpd

subzone; (c) lepidolite altering spodumene in the Mbs subzone; (d) aggregates of lepidolite, Cs-rich lepidolite, and pollucite penetrating elbaite and montebrasite in the Mbs subzone.

Abbreviations: Spd (spodumene); Mbs (montebrasite); Elb (elbaite); Lpd (lepidolite); Cs–Lpd (Cs-rich lepidolite); Pol (pollucite); Ms (muscovite); Qz (quartz); Ab (albite).

Fig. 6. Fe_T + Mg + Mn (apfu) vs F (apfu) of lepidolite in Spd, Mbs, Elb and Lpd subzones.

Fig. 7 Crystallization sequence of Li minerals in different subzones of the Nanyangshan pegmatite.

Fig. 8 Global locations of important LCT-type pegmatites, with a list of main Li minerals. References: 1 − Anderson et al. (2013); 2 − Bynoe (2014); 3 − Stilling et al. (2006) and Selway et al. (2000); 4 − Potter et al. (2009); 5 − Tindle and Breaks (2000); 6 − Sirbescu et al. (2009); 7 − Marchal et al. (2014); 8 − London and Burt (1982a); 9 − Chakoumakos and Lumpkin (1990); 10 − Kesler (1961); 11 − Shigley and Brown, JR (1985); 12 − Jolliff et al. (1987); 13 − Viana et al. (2007); 14 − Viana et al. (2007); 15 − Lagache and Quéméneur (1997); 16 − Galliski et al. (1999); 17 − Galliski et al. (2008); 18 − Oyarzábal et al. (2008); 19 – Galliski et al. (1999); 20 − Kesler et al. (2012); 21 − Badanina et al. (2015); 22 − Černý et al. (2004); 23 − Whitworth and Rankin (1989); 24 − Novák and Černý (1998); 25 − Lazić et al. (2009); 26 − Černý et al. (1989); 27 − Tonarini et al. (1998); 28 – Roda-Robles et al. (2016); 29 − Mohammedyasin (2017); 30 − Hulsbosch and Muchez (2020); 31 −

Akoh et al. (2015); 32 − Yang et al. (2020); 33 − Rijks and van der Veen (1972); 34 − Novák et al. (2015); 35 − Černý et al. (2003); 36 − Baldwin et al. (2005); 37 − Grew et al. (2018); 38 − Thomas et al. (1994); 39 − Seltmann et al. (2010); 40 − Seltmann et al. (2010); 41 − Kuznetsova and Prokof'ev (2009); 42 − Peretyazhko et al. (2004); 43 − Sokol et al. (2010); 44 − Zou and Li (2006); 45 − Peters (2011); 46 − Yin et al. (2020); 47 − this study; 48 − Matsubara et al. (1995); 49 − Liu et al. (2020); 50 − Chou and Li (2014); 51 − Li et al. (2020); 52 − Rao et al. (2017); 53 − Pal et al. (2007); Suwimonprecha et al. (1995); 55 − Sweetapple et al. (2001); 56 − Partington et al. (1995); 57 − Dittrich et al. (2014); 58 − Sweetapple et al. (2019).

Abbreviations: Ptl (petalite); Spd (spodumene); Mbs (montebrasite); Aby (amblygonite); Lhp (lithiophilite); Trp (triphylite); Elb (elbaite); Lpd (lepidolite).

Fig. 9 Comparison of the crystallization sequence of Li minerals from the Nanyangshan pegmatite with other LCT pegmatites worldwide. Li-phosphates include triphylite−lithiophilite series and montebrasite−amblygonite series.

Abbreviations: Ptl (petalite); Spd (spodumene); Elb (elbaite); Lpd (lepidolite).

852 **FIGURES**

853 Figure 1

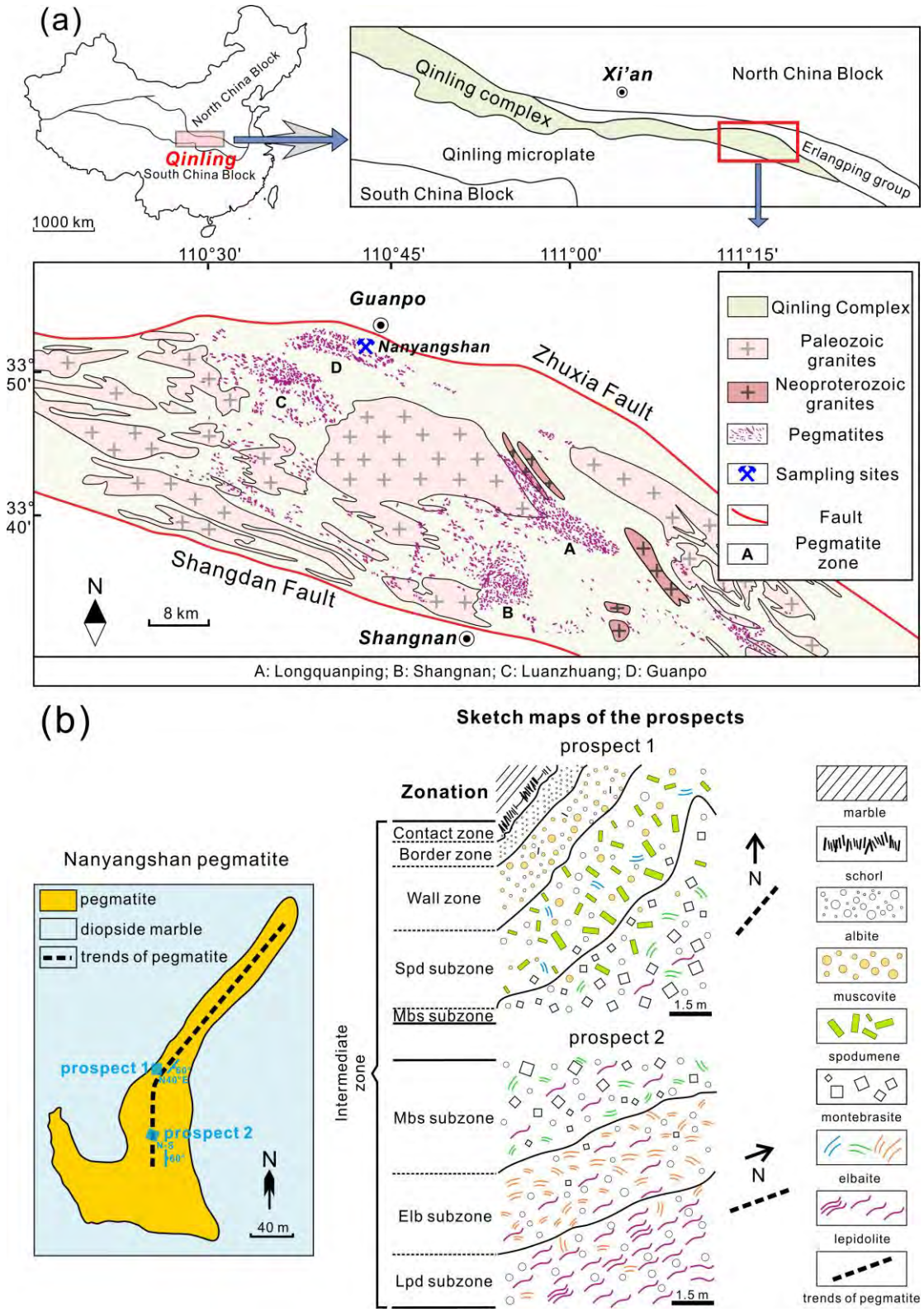

854

855

856 Figure 2

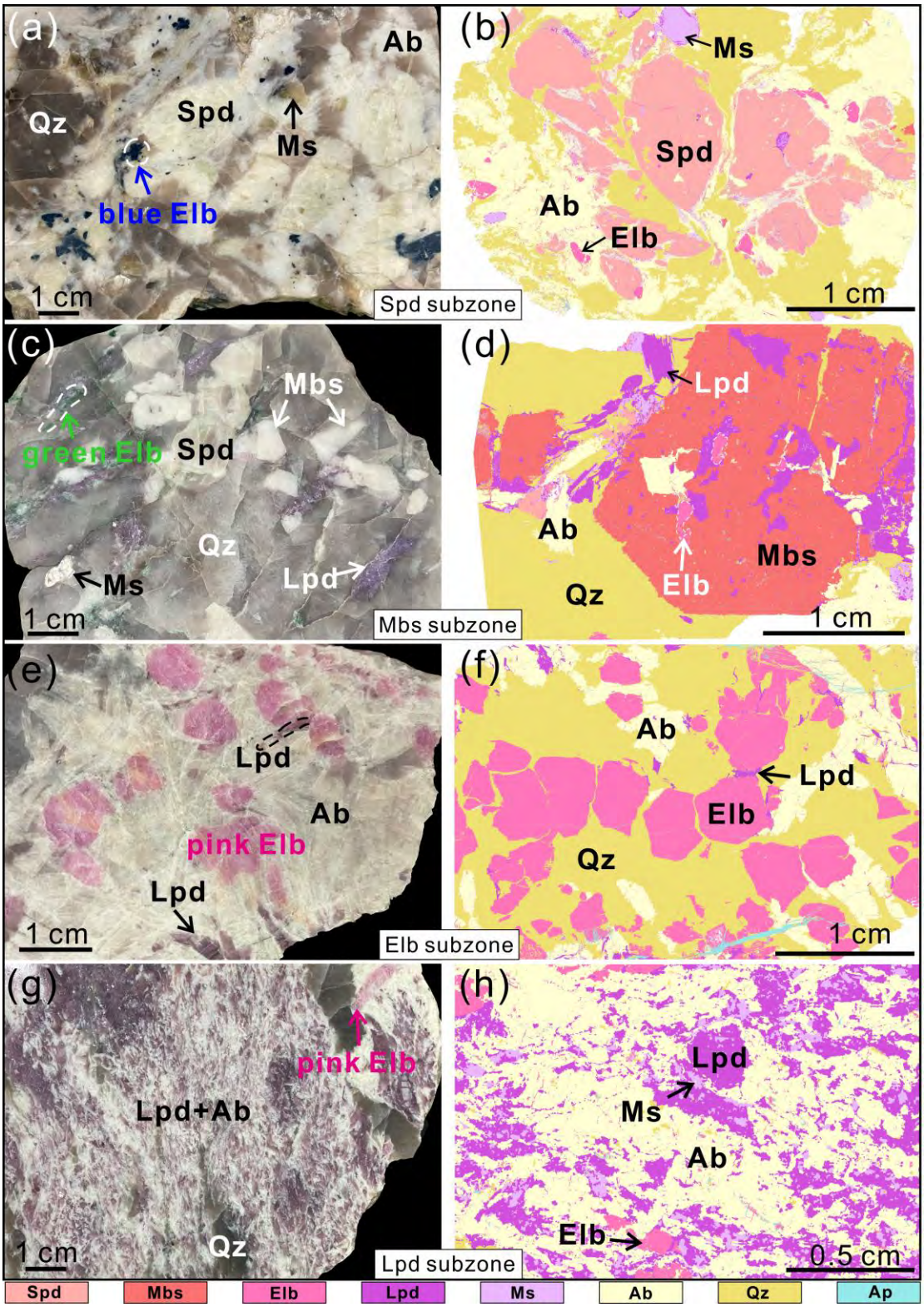

857

858

Figure 3

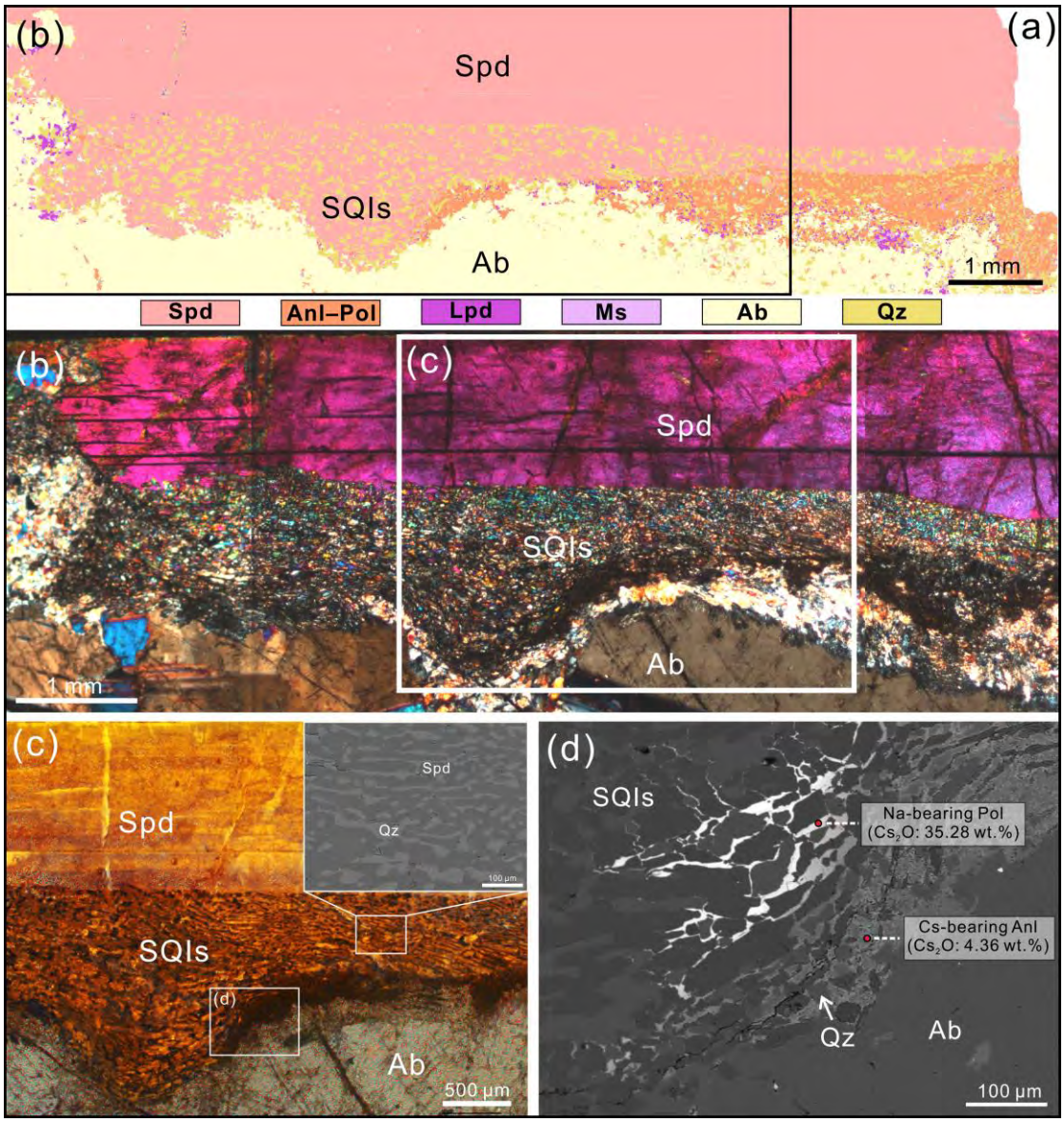

862 Figure 4

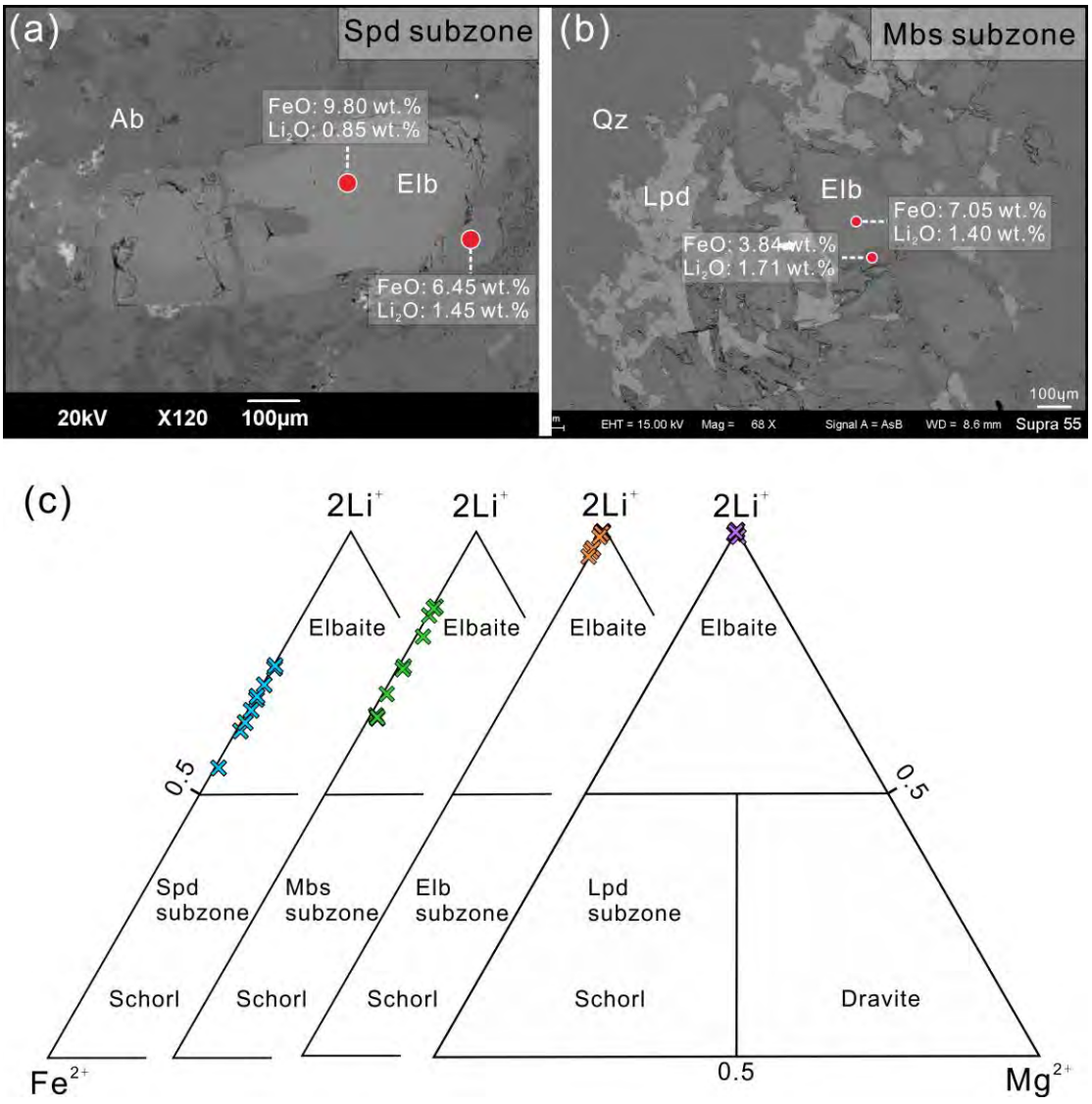

863

864

865 Figure 5

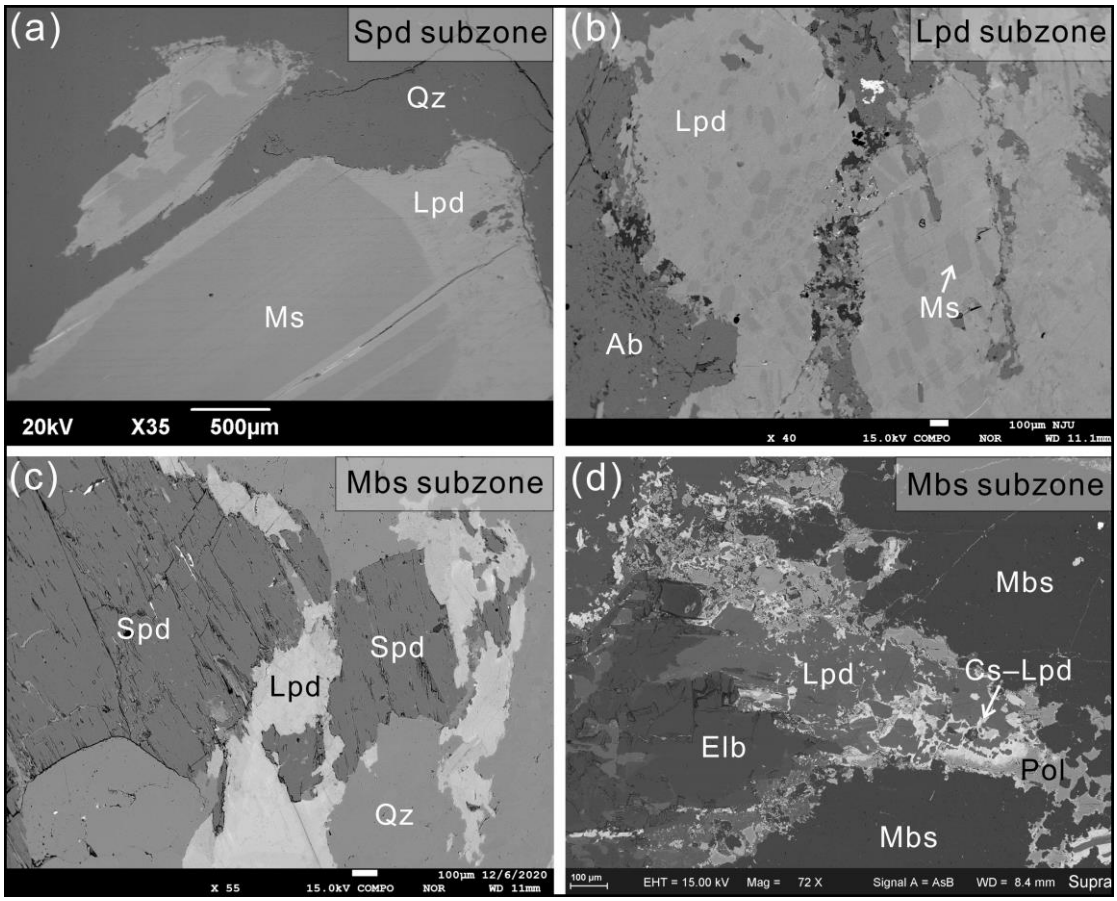

866

867

868 Figure 6

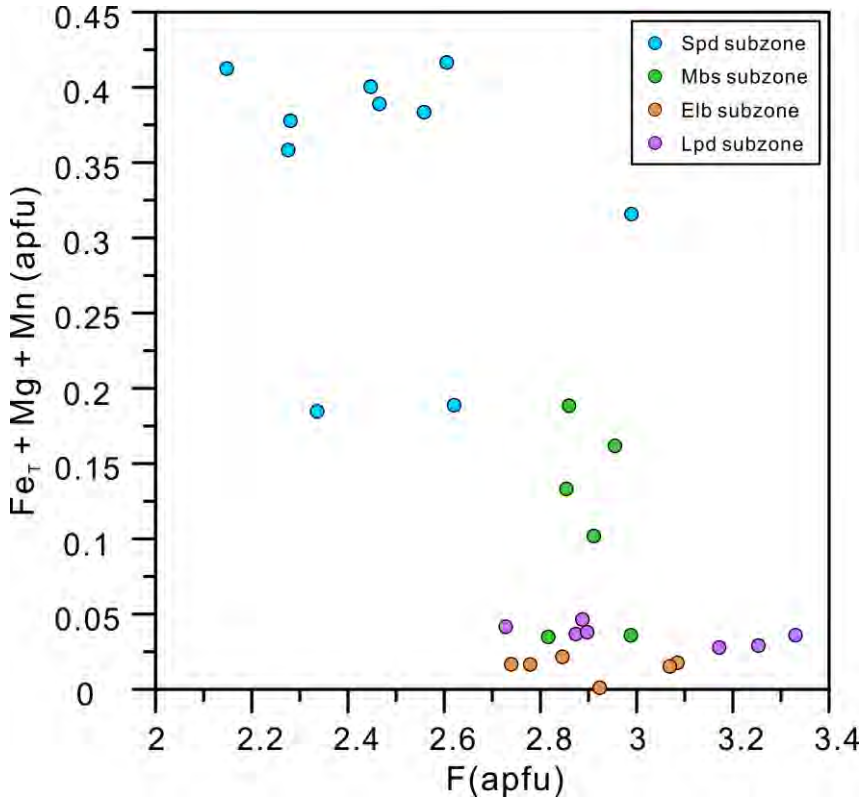

869

870 Figure 7

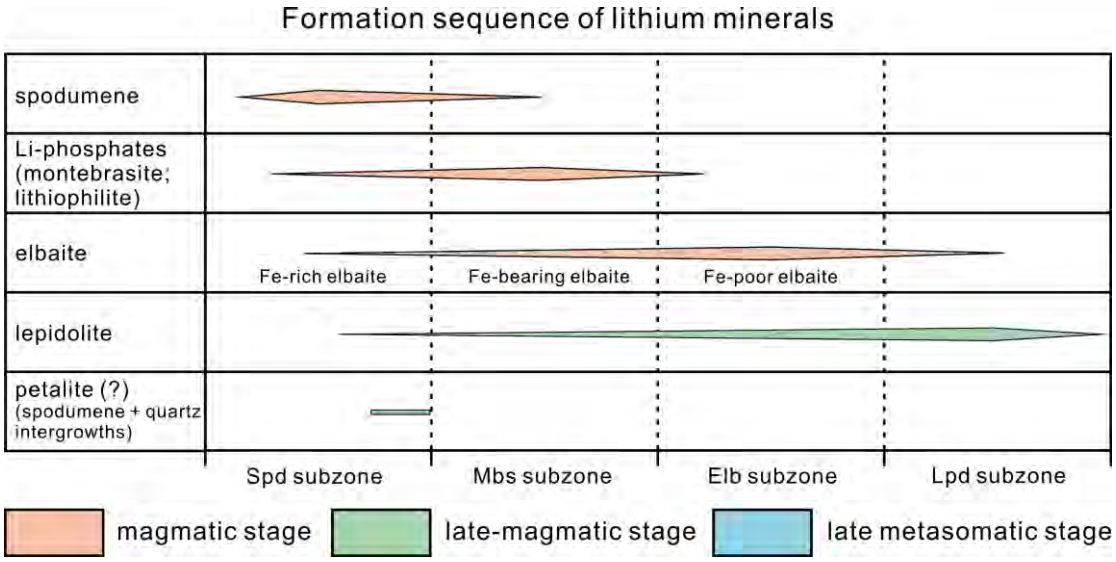

871

This is the peer-reviewed, final accepted version for American Mineralogist, published by the Mineralogical Society of America.
The published version is subject to change. Cite as Authors (Year) Title. American Mineralogist, in press.
DOI: https://doi.org/10.2138/am-2022-8285. http://www.minsocam.org/

872 Figure 8

873

874 Figure 9

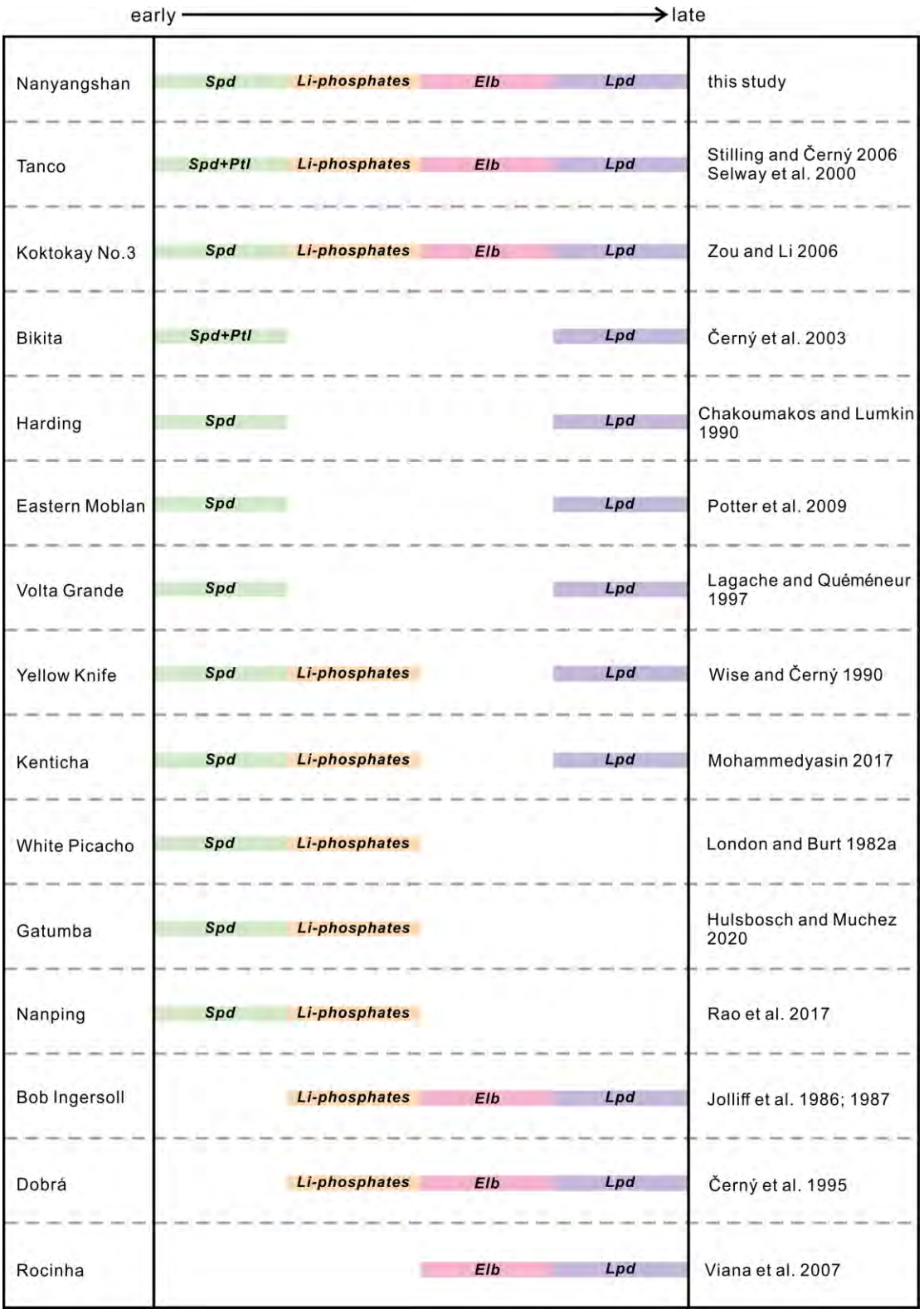

875